J Appl Electrochem (2009) 39:609–615
DOI 10.1007/s10800-008-9700-6

ORIGINAL PAPER

Sub-freezing endurance of PEM fuel cells with different catalyst-coated membranes

Wei Song · Junbo Hou · Hongmei Yu · Lixing Hao · Zhigang Shao · Baolian Yi

Received: 6 March 2008 / Accepted: 17 October 2008 / Published online: 5 November 2008

Abstract The sub-freezing endurance of proton exchange membrane (PEM) fuel cells with hydrophobic and hydrophilic catalyst-coated membranes (CCMs) was investigated. The polarization curves, electrochemical characteristics and physical structures of the CCMs were measured. The cells were frozen at −20 °C with saturated residual water after operating at 60 °C. After eight freeze/thaw cycles, no evident negative effect on the performance of the cell with a hydrophobic CCM was observed, while the cell with a hydrophilic CCM degraded severely. By analyzing the polarization curves, it was concluded that the mass transport limitation was the main reason for the performance loss of the hydrophilic cell. The electrochemical active surface area (ECA) results suggest that the hydrophobicity of the catalyst layer (CL) has an apparent impact on the residual water distribution of the membrane electrode assembly (MEA). A larger water content in the hydrophilic CL has a negative effect on the subzero endurance. From the polarization resistance obtained from electrochemical impedance spectroscopy (EIS) the origin of degradation was further clarified. Mercury intrusion porosimetry showed that the pore size of the hydrophilic catalyst layer changed significantly after freezing; the mean pore size increased from 5.68 to 6.71 nm. However, with a water removal method, namely, gas purging, it was possible to prevent degradation effectively.

W. Song · J. Hou · H. Yu (✉) · L. Hao · Z. Shao · B. Yi
Laboratory of Fuel Cells, Dalian Institute of Chemical Physics, Chinese Academy of Sciences, 457 Zhongshan Road, Dalian 116023, People's Republic China
e-mail: hmyu@dicp.ac.cn

W. Song · J. Hou · L. Hao
Graduate School of the Chinese Academy of Sciences, Beijing 100039, People's Republic China

Keywords Fuel cell · Proton exchange membrane (PEM) · Sub-freezing · Freeze/thaw · Catalyst layer · Hydrophobicity/hydrophilicity

1 Introduction

Proton exchange membrane (PEM) fuel cells are a promising substitute for internal-combustion engines for transport applications, and have attracted considerable research efforts on the cold start process and the sub-freezing endurance of the key materials. During the oxygen reduction reaction (ORR), the produced water will freeze if the temperature of the MEA is below the freezing point of water. If all the active sites in the catalyst layer (CL) are covered by ice, the fuel cell will be shut down. Moreover, during the freeze/thaw cycles, the phase transition may cause degradation to the electrode structure and cell performance. In either the cold-start process or the freeze/thaw cycles, the subzero effect of the catalyst layer is an important factor. It is possible that the structure or other characteristic of the CL may affect the cold start process as well as the sub-freezing endurance.

Modelling and experiments on the cold start process have been described in many papers [1–4]. Recently mathematic modeling studies have been implemented by Wang's group; these contribute significantly to the fundamental understanding of the cold start process [5–7]. In addition, several researchers have reported results on the freeze/thaw effect. Since the electrode structures used in the previous investigations were different, results from different papers may appear inconsistent with each other. One of the viewpoints is that the volume change due to phase transition causes material destruction or other degradation [8–10]. Cho et al. found that freeze/thaw cycles

between –10 °C and 80 °C destroy the pore distribution of the electrode and result in performance loss [8]. In their experiment a gas diffusion electrode (GDE) was used. After several cold start operations, catalyst layer delamination was observed [9]. For the GDE, it has also been reported that the electrode of a fully hydrated MEA, either as a freestanding piece or as an assembly in a cell, will be cracked after subjecting to freeze/thaw cycles between 20 °C and −30 °C [10]. The negative effect can be avoided by gas purging or other water removal methods [11, 12]. Based on these results, Hou et al. have investigated the effect of residual water on the degradation by means of electrochemical impedance spectroscopy. Their results have revealed the internal relationship between amount of water and the freezing durability of fuel cells [13]. It has also been reported that after the 100 freeze/thaw cycles from −40 °C, no performance degradation of a fuel cell was observed; in this experiment a catalyst-coated membrane (CCM) was used [14].

From the above discussion it can be seen that the sub-freezing endurance of fuel cells are dependent on electrode structure. Therefore, if the same electrode structure is used, the internal characteristic of the catalyst layer may also affect the sub-freezing endurance. The catalyst layer is significant to cell performance. According to the conventional fabrication of low platinum CLs, they can generally be classified as hydrophobic or hydrophilic. To optimize the three phase boundaries (TPB), a Nafion® solution or a polytetrafluore-ethylene (PTFE) is commonly adopted as the binder material. Hydrophobicity of a CL can be realized through heat treating and decomposing parts of the $-SO_3^+$ in Nafion®, or just by using PTFE as the binder material. Hydrophilicity of a CL can be created by using Nafion® solution as the binder material without heat treatment [15–19]. In a hydrophobic CL, the hydrophobic network is favorable for decreasing the gas transport resistance, especially when highly humid reactant gases are used. Meanwhile, overmuch hydrophobic network will impair proton transfer in the CL. In a hydrophilic CL, the Nafion® enhances the protonic conductivity of the whole CL and thus can increase the catalyst utilization. However, the possibility of water flooding in the CL is also promoted. Since the CCM shows better performance in freeze/thaw cycles, the internal nature of the CL in terms of hydrophobicity and hydrophilicity may be an underlying factor for its durability.

In this work, in order to investigate the sub-freezing endurance of fuel cells with different CL characteristics (hydrophobicity/hydrophilicity), three cells were assembled with different CCMs. Cell 1 and Cell 2 used hydrophobic and hydrophilic CCM, respectively, and they were frozen with saturated residual water. Cell 3 with a hydrophilic CCM was gas-purged before freezing. After eight freeze/thaw cycles, the cell performance, electrochemical active surface area (ECAs), and pore size distributions of the CCMs were measured, and electrochemical impedance spectroscopy (EIS) was also carried out.

2 Experimental

2.1 Fabrication of catalyst-coated membrane and MEA

A catalyst ink containing Pt/C catalyst (50%), isopropyl alcohol and Nafion® ionomer (DuPont, 5wt% solution) was sprayed onto a PTFE membrane. Then the CL was transferred onto a Nafion® 212 membrane to form a hydrophilic CCM. The fabricated CCM was pressed with a wet-proofed Toray carbon paper to form a MEA. Its effective area was 4 cm^2 and the Pt loading was 0.4 mg cm^{-2}. Similarly, the Pt loading of the hydrophobic CCM was also 0.4 mg cm^{-2} and the CCM thickness was about 50 μm. Then a MEA with this hydrophobic CCM was fabricated.

2.2 Fuel cell test and freeze/thaw cycles

Before each performance test the cells were first operated at 0.625 A cm^{-2} for 0.5 h. Pure hydrogen was used as the fuel and pure oxygen as the oxidant at a cell temperature of 60 °C. The H_2/O_2 flow rate was 40 ml min^{-1}/100 ml min^{-1} for the hydrophobic CCM cell and 80 ml min^{-1}/200 ml min^{-1} for the hydrophilic one. Such flow rate conditions ensured the cells to maintain a steady state. The operating pressures were 0.03 MPa/0.03 MPa. The humidification temperatures of the reactant gas were 60 °C/65 °C for H_2/O_2. The *i-V* curves were measured by a KFM 2030 impedance meter (Kikusui, Japan) with the Fuelcell-Load & Impedance Meter software (Kikusui, Japan). Following the *i-V* test the electrochemical impedance spectroscopy (EIS) measurements were performed. Finally, the electrochemical active area of the cell was studied with a Bi-STAT Potentiostat (USA, Princeton). The cathode was fed with N_2 at 50 ml min^{-1}, and the anode with hydrogen at 30 ml min^{-1}. When the open circuit voltage (OCV) was less than 0.1 V, cyclic voltammetry (CV) at a scan rate of 50 mV s^{-1} was carried out in the voltage range 0.05–0.8 V.

After these tests, the cell was purged with dry nitrogen gas to remove the residual water until the outlet gas humidity was about 50%. For Cells 1 and 2, a startup procedure was adopted to produce the same amount of water in the cell (as in [14]). The cell was then stored at −20 °C for 1.5 h with the outlet sealed. The cell was taken out of the climate chamber for electrochemical tests and eight cycles were repeated.

2.3 Mercury intrusion porosimetry measurements

The MEAs from the disassembled cells were dipped in ethanol, which caused the carbon paper and the CCM to separate. The porosity of the CCMs was measured by the mercury intrusion method with a PoremasterGT60 (Quantachrome). The pressure was from 1.38×10^3 to 4.13×10^7 Pa ($0.2-0.6 \times 0^4$ psi) and the mercury contact angle was 140°.

3 Results and discussion

3.1 Cell performance

To accumulate a certain amount of residual water for Cell 1 and Cell 2 before freezing, the same startup procedure was applied. However, the water-holding capacity of the two CCMs may be different due to the inherent nature of the two CCMs. An additional test was designed to measure the real amount of water. A tube filled with a desiccant was connected to the cathode outlet after the startup procedure, and the oxygen supply was switched to dry air at a flow rate of 500 ml min^{-1}. This purging process lasted for 30 min, and the water amount purged out was obtained by weighing the tube. The real water amount results were 0.30 mg for Cell 1 and 0.34 mg for Cell 2. Since the only difference between the two cells was the CCM, this phenomenon can be ascribed to the water-holding capacity difference of the two CCMs.

After operation for 0.5 h, the steady state voltages at 0.625 A cm^{-2} of Cells 1, 2 and 3 were recorded and are listed in Table 1. The "Original Cycle" stands for the initial performance: following that are the performances of the 1st, 2nd, 4th and 8th Cycle. The initial performances of the cells were different, which was probably due to the different fabrication processes and inherent nature of the two CCMs. The present investigation was focusing on the performance degradation, so the discrepancy of the initial performance could be neglected. After the 8th cycles, the voltage variation at 0.625 A cm^{-1} of Cell 1 changed from 0.640 to 0.644 V, which could be assumed as unchanged. As for Cell 2, the voltage changed from 0.538 to 0.374 V which showed obvious degradation as a result of freezing. The cell with a hydrophobic CCM showed a better freezing endurance. To clarify this point, another experiment was performed using Cell 3 with a hydrophilic CCM. Cell 3 was purged to remove the residual water before freezing. The same eight freeze/thaw cycles were carried out. The steady state voltage at 0.625 A cm^{-1} changed from 0.540 to 0.535 V implying that the cell with a hydrophilic CCM also showed a certain freezing endurance just as if the residual water was removed.

The polarization curves of the three cells during the freeze/thaw cycles are shown in Fig. 1. Similarly to the results of the steady state voltage, the *i-V* curves of Cells 1 and 2 show obviously different results. The *i-V* curve of Cell 1 was not severely affected, even in the mass transport limitation region, while that of Cell 2 degraded significantly. This degradation in the hydrophilic cell was effectively avoided by removing the residual water (Fig. 1c). Generally, the origin of fuel cell performance loss involves the ohmic resistance, the interfacial kinetic resistance and the mass transport resistance. Here, a semi-empirical equation (Eq. 1) was adopted to investigate the resistance reflected by the *i-V* curve [20, 21].

$$E = E_0 - b \log i - Ri \tag{1}$$

$$E_0 = E_r + b \log i_0 \tag{2}$$

where, E_r is the reversible potential (1.23 V), b the Tafel slope, i_0 the exchange current density for the oxygen reduction. R represents the resistance including the material bulk resistance, the interfacial contact resistance and the contribution from the mass transport limitation relating to the fitting region. The parameters can be obtained from a nonlinear least square fitting. In this work, the fitting was based on the whole *i-V* curve and the mass transport limitation contained in the R should represent the diffusion processes both in the gas diffusion layer and the catalyst layer. The values of R for the three cells are listed in Table 2.

To investigate the mass transport limitation, the ohmic resistances (R_{ohm}) of the cells obtained from electrochemical impedance spectroscopy are discussed here. Generally, this resistance depends on the proton conductivity of the PEM, the contact resistances among the electrodes, the PEM and the flow fields [2]. As shown in Table 2, the

Table 1 Steady state voltage at 0.625 A cm^{-2} of the three cells after the 0.5 h operation

Freeze/thaw cycles	Hydrophobic Cell 1 voltage/V	Hydrophilic Cell 2 voltage/V	Hydrophilic Cell 3 voltage/V
Original cycle	0.640	0.538	0.540
1st cycle	0.654	0.510	0.538
2nd cycle	0.650	0.494	0.543
4th cycle	0.640	0.467	0.524
8th cycle	0.644	0.374	0.535

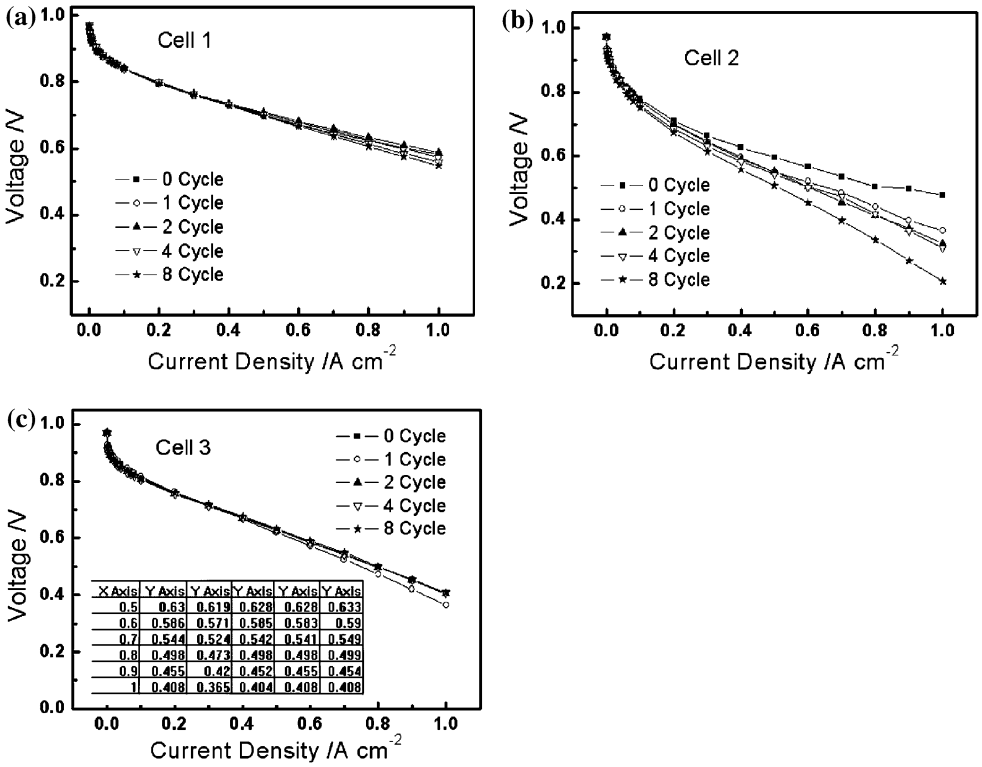

Fig. 1 Polarization curves of the three cells during the eight cycles: **a** Cell 1; **b** Cell 2; **c** Cell 3

Table 2 The ohmic resistances at 0.1 A cm^{-2} and the value of R, R-R_{ohm} and $R\%$

Freeze/thaw cycles		R_{ohm} at 0.1 A cm^{-2}/ohm cm^2	R/ohm cm^2	R-R_{ohm}/ ohm cm^2	$R\%$
Cell 1	Original cycle	0.1253	0.2310	0.1057	45.7
	4th cycle	0.1296	0.2585	0.1289	49.9
	8th cycle	0.1375	0.2695	0.1320	48.9
Cell 2	Original cycle	0.1352	0.3722	0.2370	63.7
	4th cycle	0.1475	0.5148	0.3673	71.3
	8th cycle	0.1572	0.6495	0.4923	75.8
Cell 3	Original cycle	0.1470	0.3959	0.2489	62.9
	4th cycle	0.1601	0.3907	0.2306	59.0
	8th cycle	0.1559	0.3938	0.2379	60.4

ohmic resistance of the three cells at 0.1 A cm^{-2} increased slightly after the freeze/thaw cycles. Based on ohmic resistance and the fitted R, a new resistance R-R_{ohm} is defined to study the mass transport limitation. The value of R-R_{ohm} is summarized in Table 2. The effect of the mass transport resistance on degradation may be studied with a new parameter defined as:

$$R\% = \frac{(R - R_{ohm})}{R} \times 100\% \quad (3)$$

where, $R\%$ denotes the proportion of the mass transport resistance to the total resistance, R. To a certain extent the change in $R\%$ reflects the underlying reason for performance loss. For instance, the $R\%$ of Cell 2 increased from 63.7 to 76.3% which meant that the effect of the mass transport limitation became more dominant in the total resistance after freezing. In other words, mass transport limitation must be the main reason for the freezing degradation. By comparing the change in $R\%$ for the cells, the sub-freezing storage has a more negative effect on the cell with a hydrophilic CCM with respect to the mass transport process. However, with gas purging, this effect on the hydrophilic cell disappears.

3.2 Electrochemical active surface area (ECA)

Cyclic voltammograms were measured to investigate the ECA changes after freezing, and a typical curve is shown

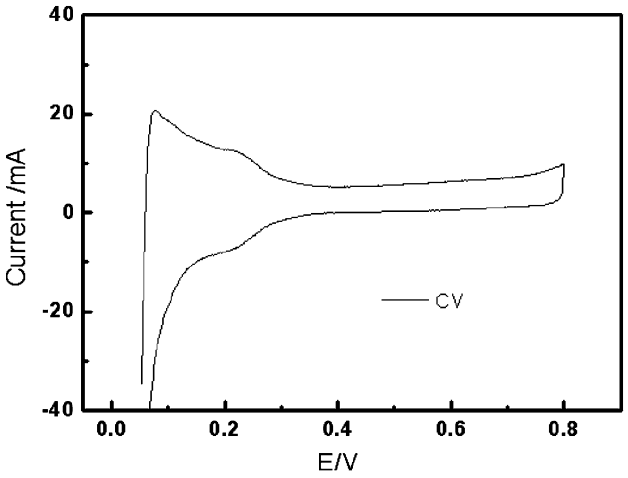

Fig. 2 Typical cyclic voltammogram of the cathode

Table 3 Sub-freezing effect on the ECA of the three cells

	Cell 1 ECA /m^2 g^{-1}	Cell 2 ECA /m^2 g^{-1}	Cell 3 ECA /m^2 g^{-1}
Original cycle	29.57	10.05	12.43
8th cycle	29.07	8.49	12.35

in Fig. 2. The ECA of a fuel cell directly reflects the condition in the CL. It stands for the active surface area where the catalyst contacts the proton conductor (electrolyte) and the electron conductor (carbon). In other words, ECA shows the resistance relating to the proton/charge transfer process and is an index of the interfacial kinetics.

The ECAs before and after the freeze/thaw cycles are listed in Table 3. The hydrophobic CCM cell showed no ECA decrease, while the ECA of the hydrophilic cell degraded by 15.5%. Since the ECA is related to the proton/charge transfer resistance, it can be concluded that the performance loss of Cell 2 is partly due to the interfacial kinetics in the CL. Taking into account Cell 3, it was found that this difference between the hydrophobic CCM and the hydrophilic CCM could be avoided if only the residual water was purged out. The results from the three cells show that the produced water in the hydrophilic CCM cell resides preferably in the CL pores compared with that in the hydrophobic CCM cell. This phenomenon has a negative effect on the electrochemical characteristics of the CL.

3.3 Electrochemical impedance spectra (EIS)

Electrochemical impedance spectroscopy of the cells was conducted to study the freezing effect. The Nyquist plots at 0.1 A cm^{-2} and 0.5 A cm^{-2} of the "Original cycle" and "8th cycle" are shown in Fig. 3. In the EIS measurement, the high frequency intercept with the real axis represents the cell resistance (ohmic resistance), and the higher frequency arc reflects the combination of an effective charge transfer resistance and a double layer capacitance within the CL. Here, the effective charge transfer resistance not only involves the charge transfer process across the catalyst/electrolyte interface but also the diffusion processes responsible for the surface concentration of the electroactive species [13, 22]. As the double layer capacitance may be assumed constant, the polarization resistance (R_p), represented by the diameter of this higher frequency arc, should contain the charge transfer resistance (R_{ct}) and internal diffusion resistance (R_{in}) in the CL.

The resistances of the three cells were fitted from the Nyquist plots and the changes are shown in Fig. 4. The R_p of the hydrophobic CCM cell shows no obvious change at both current densities, which means that neither the charge transfer resistance in the CL nor the internal diffusion resistance has increased significantly. In contrast, the hydrophilic CCM cell shows an obvious increase in R_p. The degradation of Cell 2 arises from the gas diffusion resistance and the increased proton/charge transfer resistance. The gas diffusion here includes two parts: diffusion in the gas diffusion layer (GDL) and diffusion in the CL. Hence, the EIS results can confirm that R_{ct} and R_{in} are the origin of the degradation.

3.4 Pore size distribution

Mercury intrusion porosimetry measurements were carried out to study the effect of water freezing on the pore size distribution in the CL. For comparison, the other two MEAs with hydrophobic CCM and hydrophilic CCM were used for the initial tests. These two MEAs were operated without freezing. The pore size range of the CL is strongly dependent on the fabrication procedure [23–25], and the CCMs with different structures may show a certain discrepancy. In the present investigation, the pores of the CCM lie in the range 2 to 17 nm. Since the pore size of the membrane is too small to influence the results [23, 26], the data represent the characteristics of the CL correctly. As summarized in Table 4, the mean pore diameter of the hydrophobic CCM changed from 6.82 to 6.11 nm after freezing. This means that the freezing does not affect the structure significantly. In the hydrophilic CCM, the mean pore diameter changed from 5.68 to 6.71 nm. The pore size changes of the two CCMs show that the pore expanding effect [8] in the hydrophilic CCM is more evident. Thus, it can be concluded that more water exists in the CL of the hydrophilic CCM than in the hydrophobic CCM; this has more negative effect on the CL structure. Hence, with the removal of the residual water the pore expanding effect can be eliminated.

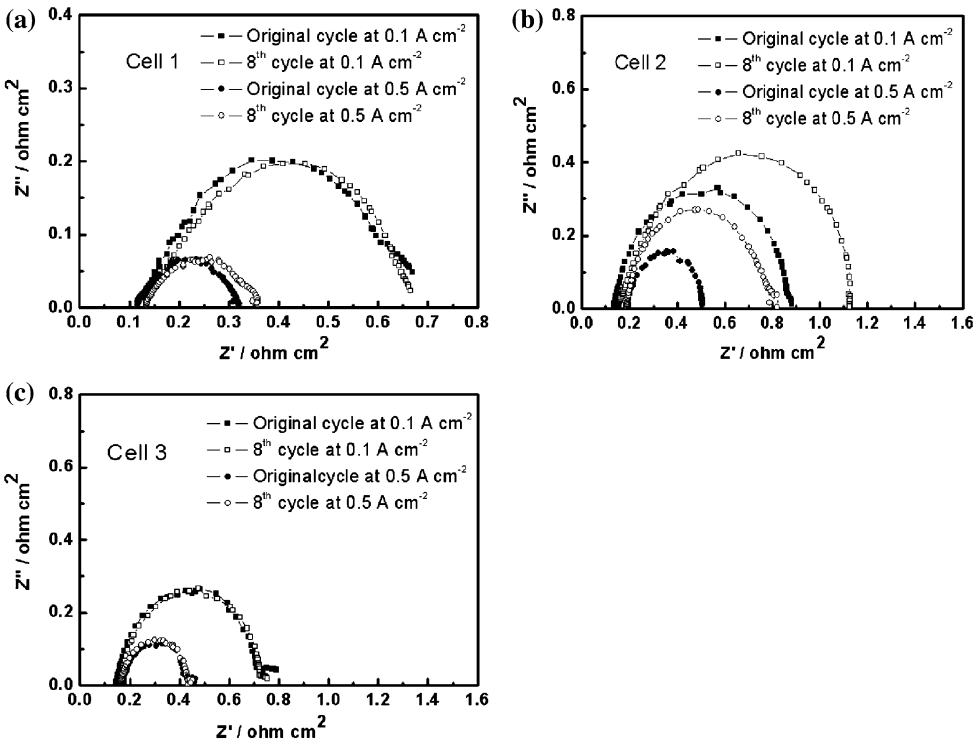

Fig. 3 The Nyquist plots at two current densities of the "Original cycle" and "8th cycle": **a** Cell 1; **b** Cell 2; **c** Cell 3

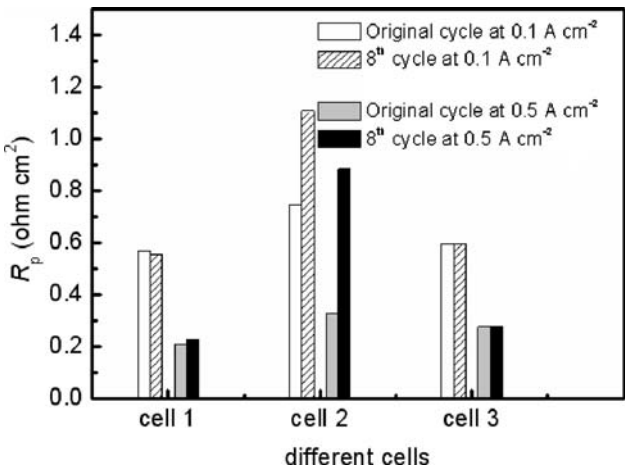

Fig. 4 Magnitude of polarization resistance obtained from the higher frequency arc in EIS

4 Conclusions

By analyzing the polarization curves during the freeze/thaw cycles of various cells, the hydrophobic cell is shown to have better sub-freezing endurance. The nonlinear least square fitting results indicate that the mass transport limitation is responsible for degradation of the hydrophilic cell. After the freezing process, the ECA of the hydrophobic cell did not decrease significantly and that of the hydrophilic cell showed a decrease of 15.5%. Since the ECA is related directly to the electrochemical characteristic of the CL, it is concluded that water remains preferentially in the CL of the hydrophilic cell compared with the hydrophobic cell. From the EIS test, the resistances relating to the CL, i.e., the charge transfer resistance and the internal diffusion resistance, have been confirmed as the origins of the degradation. Moreover, the pore size study shows that more water exists in the hydrophilic CCM and has a greater impact on the pore size changes. However, if a water removal method via gas purging is used for the hydrophilic cell, this degradation can be effectively prevented.

Table 4 The pore size data for different CCMs

Sample	Medium pore size/nm	Mean pore size/nm
Hydrophobic CCM before freezing	6.91	6.82
Hydrophobic CCM after freezing	6.18	6.11
Hydrophilic CCM before freezing	5.70	5.68
Hydrophilic CCM after freezing	6.42	6.71
Hydrophilic CCM freezing after purged	5.59	5.93

Acknowledgements This work was financially supported by the National High Technology Research and Development Program of China (863 Program, No. 2007AA11A106, No. 2007AA05Z123) and the National Natural Science Foundations of China (No. 20636060). We also thank Kikusui Electronics Crop.

References

1. Hishinuma Y, Chikahisa T, Kagami F, Ogawa T (2004) JSME Int J Ser B 47:235

2. Oszcipok M, Riemann D, Kronenwett U et al (2005) J Power Sources 145:407
3. Ahluwalia RK, Wang X (2006) J Power Sources 162:502
4. St-Pierre J, Roberts J, Colbow K et al (2005) J New Mater Electrochem Sys 8:163
5. Ge SH, Wang C-Y (2006) Electrochem Solid State Lett 9:A499
6. Mao L, Wang C-Y (2007) J Electrochem Soc 154:B139
7. Ge SH, Wang C-Y (2007) Electrochim Acta 52:4825
8. Cho EA, Ko JJ, Ha HY et al (2003) J Electrochem Soc 150:A1667
9. Guo QH, Qi ZG (2006) J Power Sources 160:1269
10. Yan QG, Toghiani H, Lee YW et al (2006) J Power Sources 160:1242
11. Cho EA, Ko JJ, Ha HY et al (2004) J Electrochem Soc 151:A661
12. Hou JB, Yu HM, Yi BL et al (2007) Electrochem Solid State Lett 10:B11
13. Hou JB, Song W, Yu HM et al (2007) J Power Sources 171:610
14. Mukundan R, Kim SY, Garzon F, Pivovar B (2005) ECS Trans 1:403
15. Wilson MS, Gottesfeld S (1992) J Appl Electrochem 22:1
16. Wilson MS, Valerio JA, Gottesfeld S (1995) Electrochim Acta 40:355
17. Gamburzev S, Appleby AJ (2002) J Power Sources 107:5
18. Gasteiger HA, Panels JE, Yan SG (2004) J Power Sources 127:162
19. Yu JR, Matsuura T, Yoshikawa Y et al (2005) Phys Chem Chem Phys 7:373
20. Ticianelli EA, Derouin CR, Redondo A, Srinivasan S (1988) J Electrochem Soc 135:2209
21. Hou JB, Yi BL, Yu HM et al (2007) Int J Hydrog Energy 32:4503
22. Ciureanu M, Roberge R (2001) J Phys Chem B 105:3531
23. Xie J, More KL, Zawodzinski TA et al (2004) J Electrochem Soc 151:A1841
24. Park HS, Cho YH, Cho YH et al (2007) Electrochim Acta 53:763
25. Uchida M, Aoyama Y, Eda N, Ohta A (1995) J Electrochem Soc 142:4143
26. Koter S (2000) J Membr Sci 166:127